Exchange interactions and temperature dependence of magnetization in half-metallic Heusler alloys

E. Şaşıoğlu,* L. M. Sandratskii,† and P. Bruno‡

Max-Planck-Institut für Mikrostrukturphysik, D-06120 Halle, Germany

I. Galanakis§

Institut of Microelectronics, NCSR "Demokritos", 15310 Aghia Paraskevi, Athens, Greece

We study the exchange interactions in half-metallic Heusler alloys using first-principles calculations in conjunction with the frozen-magnon approximation. The Curie temperature is estimated within both mean-field (MF) and random-phase-approximation (RPA) approaches. For the half-Heusler alloys NiMnSb and CoMnSb, the dominant interaction is between the nearest Mn atoms. In this case, the MF and RPA estimations differ strongly. The RPA approach provides better agreement with the experiment. The exchange interactions are more complex in the case of full-Heusler alloys Co_2MnSi and Co_2CrAl where the dominant effects are the intersublattice interactions between the Mn(Cr) and Co atoms and between Co atoms at different sublattices. For these compounds, we find that both MF and RPA give very close values of the Curie temperature slightly underestimating experimental quantities. We study the influence of the lattice compression on the magnetic properties. The temperature dependence of the magnetization is calculated using the RPA method within both quantum mechanical and classical approaches.

PACS number(s): 75.47.Np, 75.50.Cc, 75.30.Et

I. INTRODUCTION

During the last decade, the half-metallic ferromagnets have become one of the most studied classes of materials. The existence of a gap in the minority-spin band structure leads to 100% spin polarization of the electron states at the Fermi level and makes these systems attractive for applications in the emerging field of spintronics.[1] In half-metals, the creation of a fully spin-polarized current should be possible that should maximize the efficiency of magnetoelectronics devices.[2]

The half-metallicity was first predicted by de Groot and collaborators in 1983 when studying the band structure of a half-Heusler alloy NiMnSb.[3] They found that the spin-down channel is semiconducting. In 2002, Galanakis *et al.* have shown that the gap arises from the interaction between the *d* orbitals of Ni and Mn creating bonding and antibonding states separated by a gap.[4] Ishida and collaborators have proposed that also the full-Heusler compounds of the type Co_2MnZ, where *Z* stands for Si and Ge, are half-metals.[5] In these compounds, the origin of half-metallicity is more complex than in the half-Heusler alloys because of the presence of the states located entirely at the Co sites.[6] Several other Heusler alloys have been predicted to be half-metals.[7] Akinaga and collaborators[8] were able to crystallize a CrAs thin film in the zinc-blende structure, that is similar to the lattice of the Heusler alloys. The magnetic moment per formula unit was found to be close to $3\mu_B$ that corresponds to the integer value characteristic for half-metals. A number of further half-metallic materials are CrO_2 in a metastable cubic phase, Fe_3O_4, the manganites (e.g., $La_{0.7}Sr_{0.3}MnO_3$),[9] the diluted magnetic semiconductors (e.g., Mn impurities in Si or GaAs).[10,11]

Besides strong spin polarization of the charge carriers in the ground state, the spintronics materials must possess a high Curie temperature to allow the applications in the devices operating at room temperature. Available experimental information shows that the Heusler alloys are promising systems also in this respect.[12] Up to now, the main body of the theoretical studies was devoted to the properties of the half-metallic gap.[13] Recently, Chioncel and collaborators studied the influence of the correlation effects on the electron structure of CrAs.[14] They found that the spin-magnon interaction leads to the appearance of nonquasiparticle states in the spin-minority channel. The states are shown to lie above the Fermi level and to be sensitive to the value of the lattice constant. For a number of Heusler alloys it was shown that half-metallicity is preserved under tetragonalization of the crystal lattice[15] and application of the hydrostatic pressure.[16] Mavropoulos *et al.* studied the influence of the spin-orbit coupling on the spin polarization at the Fermi level and found the effect to be very small,[17] that is, in agreement with a small orbital moment calculated by Galanakis.[18] Larson *et al.*[19] have shown that the structure of Heusler alloys is stable with respect to the interchange of atoms and Orgassa and collaborators and Picozzi and collaborators have demonstrated that a small degree of disorder does not destroy the half-metallic gap.[20,21] Dowben and Skomski have shown that at nonzero temperatures, the spin-wave excitations lead to the presence at the Fermi level of the electron states with opposite spin projections leading to decreasing spin polarization of the charge carriers.[22]

Despite very strong interest to the half-metallic ferromagnetism in Heusler alloys the number of theoretical studies of exchange interactions and Curie temperature in Heusler alloys is still very small. The first contribution to the density functional theory of the exchange interactions in these systems was made in an early paper by Kübler *et al.*,[23] where the microscopic mechanisms of the magnetism of Heusler
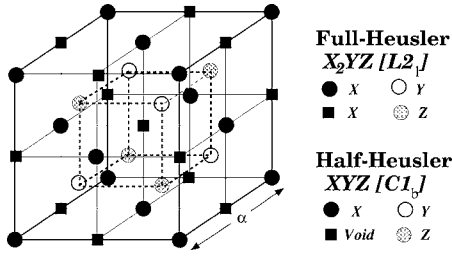
FIG. 1. $C1_b$ and $L2_1$ structures adapted by the half-Heusler and full-Heusler alloys. The lattice consists of four interpenetrating fcc lattices. In the case of the half-Heusler alloys (XYZ), one of the four sublattices is vacant. If all atoms were identical, the crystal structure would be a simple bcc lattice.

alloys were discussed on the basis of the comparison of the ferromagnetic and antiferromagnetic configurations of the Mn moments. Recently, the studies of the interatomic exchange interactions in several Heusler compounds were reported by the present authors and Kurtulus *et al.*[24–26] Şaşıoğlu *et al.* studied the exchange interactions in non-half-metallic Ni_2MnZ ($Z=Ga, In, Sn, Sb$) and half-metallic Mn_2VZ ($Z=Al, Ge$). The importance of the intersublattice exchange interaction has been demonstrated. For example, in the case of Mn_2VZ ($Z=Al, Ge$) it was shown that the antiferromagnetic coupling between the V and Mn moments stabilizes the ferromagnetic alignment of the Mn moments. Kübler[27] estimated T_C of NiMnSb to be 601 K to 701 K depending on the approach used in the calculations. These values are in good correlation with the experimental value of 730 K.[12]

The main task of the present contribution is the study of the exchange interactions in both half-Heusler and full-Heusler alloys. We use the calculated exchange parameters to estimate the Curie temperature in both the random phase (T_C^{RPA}) and the mean-field approximations (T_C^{MFA}). In Sec. II, we briefly discuss the formalism employed in the calculations. In Sec. III, we present the results on the spin-magnetic moments and the density of states (DOS) for four compounds studied: NiMnSb, CoMnSb, Co_2MnSi, and Co_2CrAl. In Sec. IV, we discuss the calculated exchange interactions and Curie temperatures. Section V is devoted to the consideration of the temperature dependence of magnetization. The films of Heusler alloys grown on different substrates can have different lattice parameters and, as a result, noticeable variation of the electron structure. Section VI contains the summary. In the Appendix, we present the formalism for the calculation of the Curie temperature of a multisublattice ferromagnet within the framework of the random-phase approximation.

II. CALCULATIONAL METHOD

Half-Heusler and full-Heusler alloys crystallize in the $C1_b$ and $L2_1$ structures, respectively (see Fig. 1). The lattice consists of four interpenetrating fcc lattices. In the case of the half-Heusler alloys (XYZ) one of the four sublattices is vacant. The Bravais lattice is in both cases fcc. In full-Heusler alloy, the atomic basis consists of four atoms. For example,

in Co_2MnSi, the positions of the basis atoms in Wyckoff coordinates are the following: Co atoms at $(0\ 0\ 0)$ and $(\frac{1}{2}\ \frac{1}{2}\ \frac{1}{2})$, Mn at $(\frac{1}{4}\ \frac{1}{4}\ \frac{1}{4})$, Si at $(\frac{3}{4}\ \frac{3}{4}\ \frac{3}{4})$. The Co atoms at the two different sublattices have the same local environment rotated by 90° with respect to the [001] axis. In half-Heusler compounds, the position $(\frac{1}{2}\ \frac{1}{2}\ \frac{1}{2})$ is vacant.

The calculations are carried out with the augmented spherical waves (ASW) method[28] within the atomic-sphere approximation (ASA).[29] The exchange-correlation potential is chosen in the generalized gradient approximation.[30] A dense Brillouin zone (BZ) sampling $30 \times 30 \times 30$ is used. The radii of all atomic spheres are chosen to be equal. In the case of half-Heusler alloys, we introduce an empty sphere located at the unoccupied site.

A. Exchange parameters

The method for the calculation of exchange constants has been presented elsewhere.[24] Here we give a brief overview.

We describe the interatomic exchange interactions in terms of the classical Heisenberg Hamiltonian,

$$H_{eff} = -\sum_{\mu,\nu} \sum_{\substack{\mathbf{R},\mathbf{R}' \\ (\mu\mathbf{R} \neq \nu\mathbf{R}')}} J_{\mathbf{R}\mathbf{R}'}^{\mu\nu} \mathbf{e}_{\mathbf{R}}^{\mu} \mathbf{e}_{\mathbf{R}'}^{\nu}. \quad (1)$$

In Eq. (1), the indices μ and ν number different sublattices and $\mathbf{R}$ and $\mathbf{R}'$ are the lattice vectors specifying the atoms within sublattices, $\mathbf{e}_{\mathbf{R}}^{\mu}$ is the unit vector pointing in the direction of the magnetic moment at site $(\mu, \mathbf{R})$.

We employ the frozen-magnon approach to calculate interatomic Heisenberg exchange parameters.[31] The calculations involve few steps. In the first step, the exchange parameters between the atoms of a given sublattice μ are computed. The calculation is based on the evaluation of the energy of the frozen-magnon configurations defined by the following atomic polar and azimuthal angles

$$\theta_{\mathbf{R}}^{\nu} = \theta, \quad \phi_{\mathbf{R}}^{\nu} = \mathbf{q} \cdot \mathbf{R} + \phi^{\nu}. \quad (2)$$

The constant phase ϕ^{ν} is chosen to be equal to zero. The magnetic moments of all other sublattices are kept parallel to the z axis. Within the Heisenberg model (1), the energy of such configuration takes the form

$$E^{\mu\mu}(\theta, \mathbf{q}) = E_0^{\mu\mu}(\theta) + \sin^2 \theta J^{\mu\mu}(\mathbf{q}), \quad (3)$$

where $E_0^{\mu\mu}$ does not depend on $\mathbf{q}$ and the Fourier transform $J^{\mu\nu}(\mathbf{q})$ is defined by

$$J^{\mu\nu}(\mathbf{q}) = \sum_{\mathbf{R}} J_{0\mathbf{R}}^{\mu\nu} \exp(i\mathbf{q} \cdot \mathbf{R}). \quad (4)$$

In the case of $\nu = \mu$, the sum in Eq. (4) does not include $\mathbf{R} = 0$. Calculating $E^{\mu\mu}(\theta, \mathbf{q})$ for a regular $\mathbf{q}$-mesh in the Brillouin zone of the crystal and performing back-Fourier transformation, one gets exchange parameters $J_{0\mathbf{R}}^{\mu\mu}$ for sublattice μ. The determination of the exchange interactions between the atoms of two different sublattices μ and ν is discussed in Ref. 24.

TABLE I. Calculated atom-resolved and total spin moments in μ_B for NiMnSb, CoMnSb, Co$_2$CrAl, and Co$_2$MnSi. All compounds are half-metallic at the experimental lattice constants taken from Ref. 12. a_{II} means the use of the lattice constant that places the Fermi level at the upper edge of the half-metallic gap and a_{III} corresponds to 1% contraction of the lattice constant with respect to a_{II}.

Compound	a(Å)	X	Y	Z	Void	Total
NiMnSb—$a_{I[exp]}$	5.93	0.20	3.85	−0.09	0.04	4.00
NiMnSb—a_{II}	5.68	0.32	3.68	−0.05	0.05	4.00
NiMnSb—a_{III}	5.62	0.33	3.64	−0.04	0.05	3.97
CoMnSb—$a_{I[exp]}$	5.87	−0.32	3.41	−0.11	0.02	3.00
CoMnSb—a_{II}	5.22	0.45	2.57	−0.06	0.04	3.00
CoMnSb—a_{III}	5.17	0.48	2.52	−0.05	0.04	2.99
Co$_2$CrAl—$a_{I[exp]}$	5.74	0.62	1.83	−0.08	—	3.00
Co$_2$CrAl—a_{II}	5.55	0.69	1.68	−0.06	—	3.00
Co$_2$CrAl—a_{III}	5.49	0.69	1.66	−0.05	—	2.99
Co$_2$MnSi—$a_{I[exp]}$	5.65	0.93	3.21	−0.06	—	5.00
Co$_2$MnSi—a_{II}	5.49	0.97	3.10	−0.04	—	5.00
Co$_2$MnSi—a_{III}	5.43	0.97	3.01	−0.04	—	4.97

B. Curie temperature

The Curie temperature is estimated within two different approaches: the mean-field approximation (MFA) and random-phase approximation (RPA). The MFA for a multi-sublattice material requires solving the system of coupled equations[24,32]

$$\langle e^\mu \rangle = \frac{2}{3k_B T} \sum_\nu J_0^{\mu\nu} \langle e^\nu \rangle, \quad (5)$$

where $\langle e^\nu \rangle$ is the average z component of $\mathbf{e}_\mathbf{R}^\nu$ and $J_0^{\mu\nu} \equiv \Sigma_\mathbf{R} J_{0\mathbf{R}}^{\mu\nu}$. Equation (5) can be represented in the form of an eigenvalue matrix problem

$$(\mathbf{\Theta} - T\mathbf{I})\mathbf{E} = 0, \quad (6)$$

where $\Theta_{\mu\nu} = 2/3k_B J_0^{\mu\nu}$, $\mathbf{I}$ is a unit matrix, and $\mathbf{E}$ is the vector of $\langle e^\nu \rangle$. The largest eigenvalue of matrix Θ gives the value of T_C^{MFA}.[32]

A more consequential method for the study of the thermodynamics of Heisenberg systems is provided by the RPA approach.[33,34] The RPA technique is intensively used for studies of both single-sublattice[35,36] and multisublattice[37–45] systems. In the case that only the exchange interactions within one sublattice are important, the Curie temperature within the RPA is given by the relation[35]

$$\frac{1}{k_B T_C^{RPA}} = \frac{3}{2} \frac{1}{N} \sum_q \frac{1}{J(\mathbf{0}) - J(\mathbf{q})}. \quad (7)$$

We use the RPA approach to study the temperature dependence of the magnetization in the temperature interval from 0 K to T_C. The RPA technique for a multisublattice system is briefly presented in the appendix.

III. DOS AND MAGNETIC MOMENTS

A. NiMnSb and CoMnSb

In this section, we report the calculation of DOS and magnetic moments at different lattice parameters for NiMnSb and for a CoMnSb compound that has one electron per formula unit less than NiMnSb. The electronic structure of both compounds has been extensively studied earlier and the reader is referred to Ref. 49 and references therein for a detailed discussion. Here we present a brief description of the calculational results aiming to provide the basis for further considerations and to allow the comparison with previous work.

In Table I, we collect the atomic and total spin moments for three different lattice parameters. The investigation of the influence of the value of the lattice parameter on the properties of the Heusler alloys is important since the samples grown on different substrates can have different lattice spacings. The first calculation is performed for the experimental bulk lattice constant.[12] The calculated densities of states (DOSs) for this case are presented in the upper panel of Fig. 2. For both NiMnSb and CoMnSb, the Fermi level lies in the low-energy part of the half-metallic gap. The compression of the lattice pushes the majority p states to higher energies that results in increased energy position of the Fermi level with respect to the half-metallic gap. At the lattice parameter a_{II}, the Fermi level coincides with the upper edge of the gap (Fig. 2). In the next step, we further contracted the lattice constant by 1% (lattice parameter a_{III}, bottom panel in Fig. 2). In this case, the Fermi level is slightly above the gap and the total spin moment is slightly smaller than the integer values of $3\mu_B$ and $4\mu_B$ for CoMnSb and NiMnSb, respectively.

The contraction of the lattice leads to an increase of the hybridization between the d orbitals of different transition-metal atoms. This results in a decrease of the spin moment of
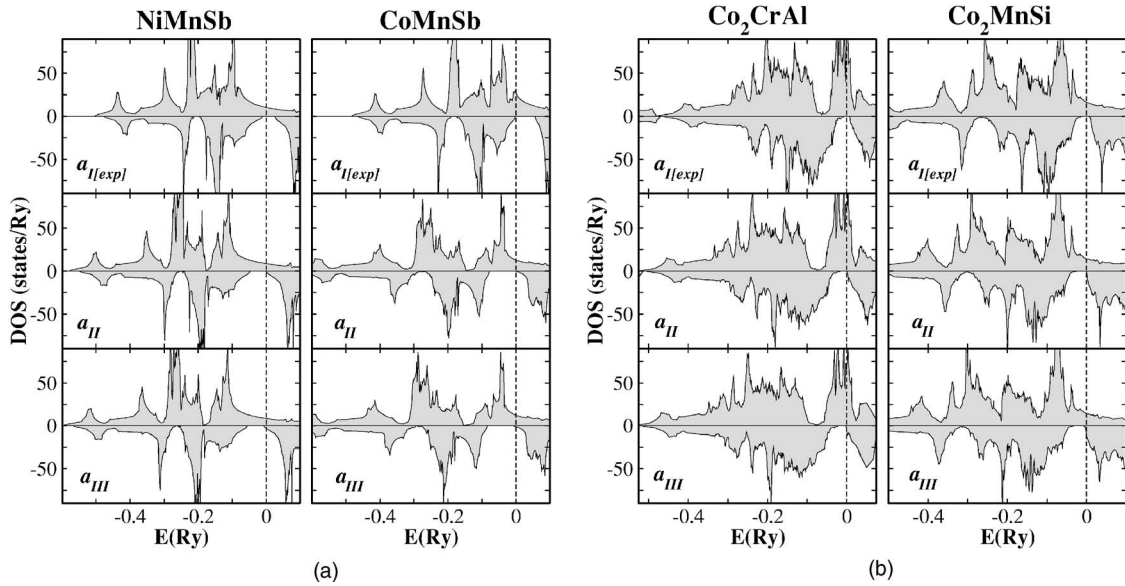
FIG. 2. (a) Calculated spin-resolved density of states of NiMnSb and CoMnSb for three values of the lattice parameter. (b) The same for Co_2CrAl and Co_2MnSi. The upper panels present the results for the experimental lattice constant (Ref. 12). The middle panels show the results for the lattice parameter a_{II} that is determined by the coincidence of the Fermi level with the upper edge of the half-metallic gap. The bottom panels present the results for lattice parameter a_{III} that is obtained by a 1% contraction of a_{II}.

Mn. In the case of NiMnSb, this change is small: the reduction of the Mn spin moment under lattice contraction from the experimental lattice parameter to a_{II} is $\sim 0.2\mu_B$. The Ni spin moment increases by about the same value to preserve the integer value of the total spin moment of $4\mu_B$.

In CoMnSb, the half-metallic gap is larger than in NiMnSb. As a result, the transition of the Fermi level to the upper gap edge requires a large lattice contraction of 11% (Table I). This leads to a strong decrease of the Mn moment by $0.84\mu_B$. To compensate this decrease, the Co moment changes its sign transforming the magnetic structure from ferrimagnetic to ferromagnetic.

The influence of the lattice contraction on the exchange interactions and Curie temperature is discussed in Sec. IV.

B. Co_2CrAl and Co_2MnSi

The second group of materials studied in the paper is formed by the full-Heusler compounds Co_2MnSi and Co_2CrAl. The electronic structure of these systems has been studied earlier.[6] Compared to half-Heusler systems, the presence of two Co atoms per formula unit results in an increased coordination number of Co atoms surrounding Mn atoms (eight instead of four in CoMnSb). This leads to an increased hybridization between the $3d$ orbitals of the Mn and Co atoms. The spin moment of Co in Co_2MnSi is about $1\mu_B$ that is considerably larger than the Co moment in CoMnSb. In Co_2CrAl, the Co moment is about one-third smaller than in Co_2MnSi that reflects a smaller value of the Cr moment compared to the Mn moment (Table I).

As in the case of the half-Heusler compounds discussed above, the variation of the lattice parameter leads to the change in the position of the Fermi level. At the experimental lattice parameter, the Fermi level of Co_2CrAl lies in the

lower part of the half-metallic gap while for Co_2MnSi it is close to the middle of the gap [Fig. 2(b)]. The contraction of the lattice needed to place the Fermi level at the upper edge of the gap is smaller than for CoMnSb. As a result, the change in the magnetic moments is also relatively weak (Table I).

IV. EXCHANGE PARAMETERS AND CURIE TEMPERATURE

A. NiMnSb and CoMnSb

In Fig. 3, we present the exchange constants calculated for various lattice spacings. The Co-Co, Ni-Ni exchange interactions, as well as the exchange interactions between the moments of the $3d$ atoms and the induced moments of Sb atoms, are very weak and are not shown. The weakness of the effective Co-Co and Ni-Ni exchange interactions can be explained by a relatively large distance between atoms (Fig. 1) and relatively small atomic moments.

On the other hand, each Ni(Co) atom is surrounded by four Mn atoms as nearest neighbors that results in strong Mn-Ni(Co) exchange interaction (Fig. 3). Also the exchange interaction between large Mn moments is strong.

The ferromagnetic Mn-Mn interactions are mainly responsible for the stable ferromagnetism of these materials. For both systems and for all lattice spacings studied, the leading Mn-Mn exchange interaction is strongly positive. In NiMnSb, the Mn-Ni interaction of the nearest neighbors is positive for all three lattice parameters leading to the parallel orientation of the spins of the Mn and Ni atoms. In CoMnSb, the situation is different. At the experimental lattice parameter, the leading Mn-Co interaction is negative, resulting in the ferrimagnetism of the system. For the contracted lattices,
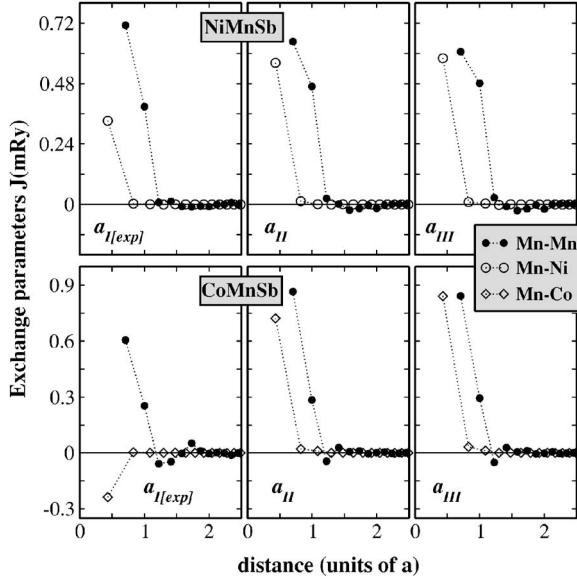
FIG. 3. The variation of the interatomic exchange parameters for NiMnSb (upper panel) and CoMnSb (bottom panel) as a function of the interatomic distance. The left panel corresponds to the experimental lattice constant, the middle and right panels correspond respectively to a_{II} and a_{III} parameters.

TABLE II. Calculated Curie temperatures. The second and third columns contain the $T_C^{MFA(RPA)}$ obtained with the account for Mn-Mn (Cr-Cr) interactions only. In the next two columns, all interactions are taken into account. The last column presents the experimental values of the Curie temperature from Ref. 12.

T_C (K)	MFA-Y	RPA-Y	MFA-all	RPA-all	Exp.
NiMnSb—$a_{I[exp]}$	1096	880	1112	900	730
NiMnSb—a_{II}	1060	853	1107	908	—
NiMnSb—a_{III}	1008	802	1063	869	—
CoMnSb—$a_{I[exp]}$	785	619	815	671	490
CoMnSb—a_{II}	1185	940	1276	1052	—
CoMnSb—a_{III}	1140	893	1252	1032	—
Co$_2$CrAl—$a_{I[exp]}$	148	141	280	270	334
Co$_2$CrAl—a_{II}	168	159	384	365	—
Co$_2$CrAl—a_{III}	164	154	400	379	—
Co$_2$MnSi—$a_{I[exp]}$	232	196	857	740	985
Co$_2$MnSi—a_{II}	142	118	934	804	—
Co$_2$MnSi—a_{III}	110	75	957	817	—

the interaction changes sign, resulting in the ferromagnetic ground state of the alloy.

The analysis of the strength of the exchange interaction as a function of the lattice parameter shows that in CoMnSb, the contraction leads to a strong increase of both leading Mn-Co and Mn-Mn interactions. On the other hand, in NiMnSb, the increase of the Mn-Ni interaction is accompanied by a decrease of the leading Mn-Mn interaction. Simultaneously, the interaction between the second-nearest Mn atoms increases with contraction in the case of NiMnSb staying almost unchanged in CoMnSb. This complexity of the behavior reflects the complexity of the electronic structure of the systems.

The interatomic exchange parameters are used to evaluate the Curie temperature within two different approaches: MFA and RPA. In Table II, we present the values of the Curie temperature obtained, first, by taking into account the Mn-Mn interactions only and, second, with account for both Mn-Mn and Mn-Ni(Co) interactions. The contribution of the intersublattice interactions to the Curie temperature appears to be less than 5% for both compounds and the Curie temperature is mainly determined by the intrasublattice Mn-Mn interaction.

The MFA and RPA estimations of the Curie temperature differ rather strongly (Table II). The relative difference of two estimations is about 20%. The reason behind this difference will be discussed in Sec. V. For the systems considered here, the RPA estimations of the Curie temperatures are in good agreement with the experiment, somewhat overestimating the experimental values.

Recently, Kübler[27] reported estimations of the Curie temperature of NiMnSb. His approach is based on the evaluation of the nonuniform magnetic susceptibility on the basis of the Landau-type expansion for the free energy. Within some ap-

proximations, the parameters used in the study of the thermodynamical properties can be expressed in terms of the quantities evaluated within the first-principles density functional theory (DFT) calculations. The estimated values of the Curie temperature are 601 K for a static approach and 701 K if the frequency dependence of the susceptibility is taken into account. These estimations are somewhat lower than the value of 880 K given by the RPA approach (Table II). A detailed comparative analysis of the two calculational schemes is needed to get an insight in the physical origin of this difference.

The contraction of the lattice in the case of the NiMnSb compound leads to an increase of the Mn-Ni interactions (Fig. 3). This results in increased difference between the Curie temperatures calculated with the Mn-Mn interactions only and with both Mn-Mn and Ni-Mn interactions taken into account (Table II). For CoMnSb, the leading exchange interactions of both Mn-Mn and Mn-Co types increase in the value under transition from the experimental lattice constant to a_{II} (Fig. 3). As a result, the Curie temperature increases with contraction by about 50%.

B. Co$_2$CrAl and Co$_2$MnSi

The presence of an extra Co atom in the full-Heusler alloys makes the interactions more complex than in the case of the half-Heusler alloys. In CoMnSb, the important interactions arise between nearest Mn atoms (Mn-Mn interactions) and between nearest Mn and Co atoms (Mn-Co interaction). In the case of Co$_2$MnSi (Fig. 4) the interactions between Co atoms at the same sublattice (Co-Co) and between Co atoms at different sublattices (Co^1-Co^2) must be taken into account. The cobalt atoms at different sublattices have the same local environment rotated by 90° about the [001] axis. The leading interaction responsible for the stability of the
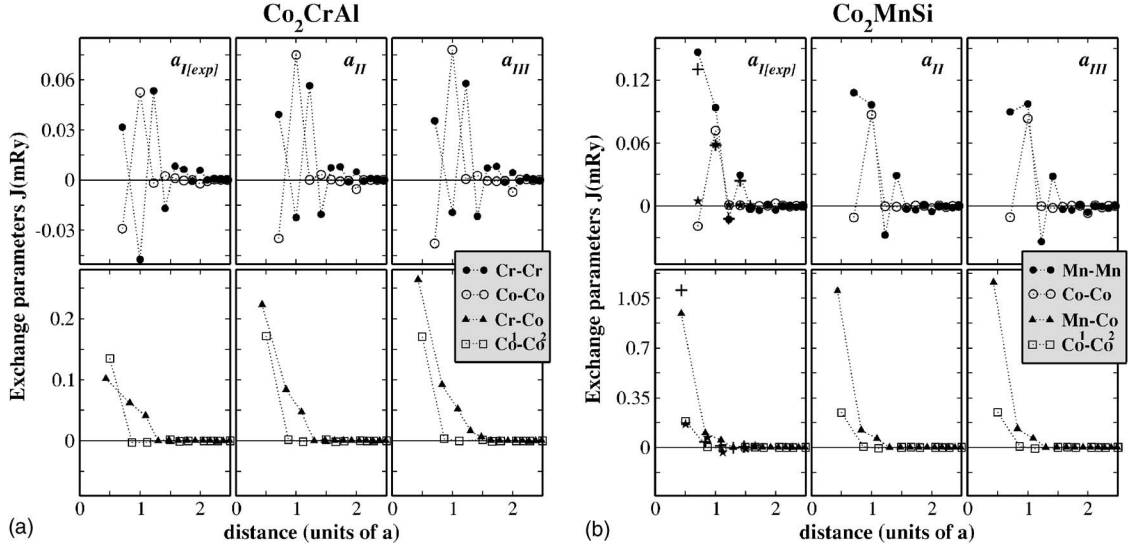
FIG. 4. (a) The exchange constants for Co_2CrAl as a function of the interatomic distance. (b) The same for Co_2MnSi. The left panels correspond to the experimental lattice constant, the middle and right panels to a_{II} and a_{III} parameters, respectively. The superscripts 1 and 2 denote Co atoms belonging to different sublattices (Fig. 1). For comparison, the exchange parameters of Co_2MnSi obtained in Ref. 26 at the experimental lattice parameter ($a_I[exp]$) are shown. The following symbols are used in the presentation: + for the Mn-Mn and Mn-Co interactions and ⋆ for the Co-Co and Co^1-Co^2 interactions.

ferromagnetism is the Mn-Co interaction between Mn atoms and the eight nearest Co atoms (Fig. 4). This interaction changes weakly with the contraction of the lattice. Our exchange parameters agree well with the parameters of Kurtulus *et al.* (Fig. 4) who also found the Co-Mn exchange interaction to be leading.[26]

The interaction between nearest Co atoms at different sublattices (empty squares in Fig. 4) favors the ferromagnetism also and is stronger than the ferromagnetic interaction between the nearest Mn atoms (filled spheres). Although the spin moment of Mn atoms is larger than the moment of Co atoms (Table I) the opposite relation between exchange parameters can be the consequence of the smaller distance between the Co atoms: $a/2$ between the Co atoms and $\sqrt{2}a/2$ between the Mn atoms. An interesting feature of the intrasublattice Mn-Mn and Co-Co interactions is different signs of the exchange parameters for different distances between atoms. This leads to a Ruderman-Kittel-Kasuya-Yosida (RKKY)-like oscillations of the parameters (Fig. 4).

In Co_2CrAl, the leading Cr-Co interactions (filled triangles) are much smaller than corresponding Mn-Co interactions in Co_2MnSi. On the other hand, the leading intersublattice ferromagnetic Co-Co interactions are comparable in both systems. The compression of the lattice leads to an increase of the magnitude of the intersublattice Co-Cr and Co^1-Co^2 coupling. The intrasublattice Cr-Cr and Co-Co interactions oscillate with varying interatomic distances.

The difference in the properties of the exchange parameters of the half-Heusler and full-Heusler alloys is reflected in the calculated Curie temperatures (Table II). In contrast to CoMnSb where the Mn-Mn exchange interactions are dominant, in Co_2MnSi they play a secondary role. The $T_C^{MFA(RPA)}$ calculated taking into account these interactions only is much smaller than the Curie temperature calculated with all interatomic exchange interactions taken into account (Table

II). The same conclusion is valid for Co_2CrAl where the Cr-Cr interactions give about half of the Curie temperature obtained with all interactions included into consideration.

A striking feature of the full Heusler compound Co_2CrAl that differs it strongly from the half-Heusler systems considered in Sec. III is a very small difference between the T_C values calculated within the MFA and RPA approaches. A similar behavior was obtained for the Curie temperatures of the zinc-blende MnSi and MnC.[46] In Co_2MnSi, the relative difference of the MFA and RPA estimations assumes an intermediate position between the half-Heusler systems and Co_2CrAl.

To understand the origin of the strong variation of the relative difference of the MFA and RPA estimations of the Curie temperature, we compare in Fig. 5 the frozen-magnon dispersions for two compounds. The magnons correspond to the Mn sublattice in the case of NiMnSb and to the Cr sublattice in the case of Co_2CrAl. As seen from Table II, the MFA and RPA estimations obtained with the use of these dispersions differ by 20% for NiMnSb and by 5% for Co_2CrAl.

The Curie temperature is given by the average value of the magnon energies. In MFA this is the arithmetic average, while in RPA this is the harmonic average. Therefore, we need to understand why for Co_2CrAl these two averages are much closer than for NiMnSb. The following properties of the averages are important for us. The arithmetic average takes all the magnon values with equal weight whereas in the harmonic average, the weight decreases with increasing energy of the magnon.[35,36,46–48] It is an arithmetic property that the MFA estimation is larger than the RPA one or equal to it if all numbers to be averaged are equal to each other. In terms of magnon energies, T_C^{MFA} is equal to T_C^{RPA} in the case that the magnon spectrum is dispersionless.

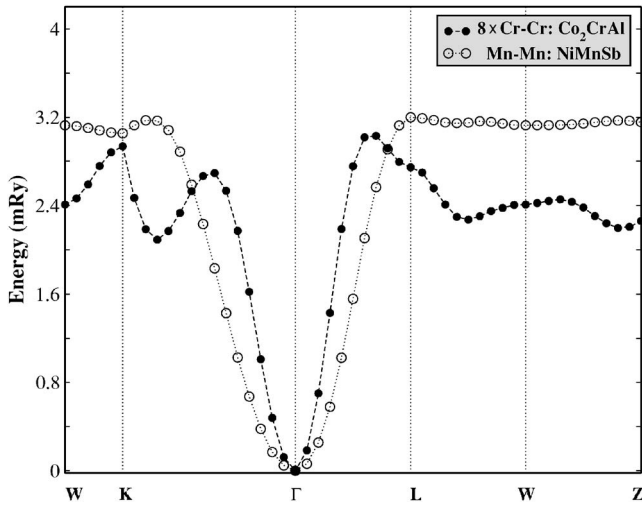Considering the frozen-magnon dispersions from the viewpoint of these properties, we indeed can expect that the

FIG. 5. The frozen-magnon dispersions for NiMnSb and Co_2CrAl along the symmetry lines in the Brillouin zone. The magnons correspond to the Mn sublattice in the case of NiMnSb and to the Cr sublattice in the case of Co_2CrAl. For Co_2CrAl, the frozen-magnon energies are multiplied by a factor of 8.

arithmetic and harmonic averages will be closer for Co_2CrAl. In Fig. 5, both curves are scaled to have almost the same maximal value. It is seen that the Co_2CrAl dispersion has smaller relative contribution of the low-energy magnons because of the steeper increase of the curve at small wave vectors. It has also smaller contribution of the magnons with the largest energies because the maxima have the form of well-defined peaks opposite to NiMnSb where we get a plateau. Thus, the main contribution in the case of Co_2CrAl comes from intermediate energies that makes the MFA and RPA estimations closer.

In Fig. 6, we present the calculated spin-wave spectra for NiMnSb and Co_2CrAl. The spin-wave energies are obtained by the diagonalization of the matrix of exchange parameters that contains all the important intrasublattice and intersublattice interactions. The number of branches in the spectrum is equal to the number of magnetic atoms in the unit cell: two in NiMnSb and three in Co_2CrAl. One of the branches is acoustic and has zero energy for the zero wave vector. Also in the spin-wave spectra, we see a strong difference between two systems. In NiMnSb, the acoustic branch is predominantly of the Ni type stemming from the weak interaction between Mn and Ni magnetic moments (see Fig. 3). On the other hand, the optical branch is of predominantly the Mn type. The strong hybridization between two sublattices is obtained at only about $\mathbf{q}=0$. In Co_2CrAl, the energy scale of the branches differs much smaller and the hybridization between sublattices is stronger than for NiMnSb.

Coming back to the considerations of the Curie temperatures, we conclude that, in general, the Curie temperatures of Co_2MnSi and Co_2CrAl calculated within both MFA and RPA are in good agreement with experiment while the MFA values in the case of NiMnSb and CoMnSb overestimate the Curie temperature strongly.

The lattice contraction leads in both compounds to an enhancement of the Mn‑Co(Cr‑Co) exchange constants that
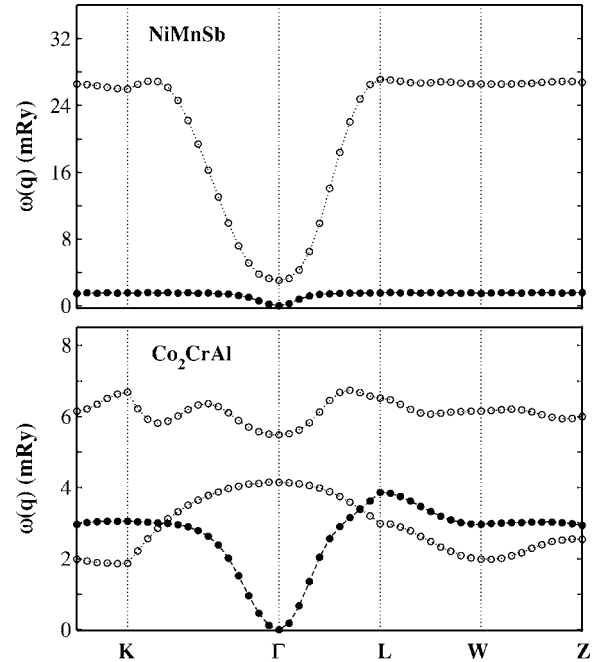

FIG. 6. The spin-wave dispersions for NiMnSb and Co_2CrAl along the symmetry lines in the Brillouin zone. Filled and empty spheres denote the acoustic and optical branches, respectively.

results in an increase of the Curie temperature.

Kurtulus and collaborators have calculated the Curie temperature for Co_2MnSi within MFA and found the value of 1251 K that is considerably larger than our MFA estimate of 857 K. This difference is unexpected since the values of the exchange parameters obtained by Kurtulus *et al.* agree well with our parameters (Fig. 4). To reveal the origin of the discrepancy, we performed the MFA calculation of the Curie temperature with the exchange parameters of Kurtulus *et al.* and obtained the T_C value of 942 K which is in reasonable agreement with our estimate. Apparently the reason for the inconsistency is in the procedure of the solving of the multiple-sublattice MFA problem used by Kurtulus *et al.* that should deviate from the standard one.[32]

V. TEMPERATURE DEPENDENCE OF THE MAGNETIZATION

The study of the temperature dependence of the magnetic properties of itinerant ferromagnets is one of the fundamental problems of ongoing researches.[50] Although density functional theory can formally be extended to the finite temperatures,[51] it is rarely used because of the lack of suitable exchange-correlation potentials for magnetic systems at finite temperatures. Statistical mechanics treatment of model Hamiltonians is usually employed. In this section, we will present the results of the calculation of the temperature dependence of magnetization that is based on the consideration of the Heisenberg Hamiltonian with exchange parameters calculated within a parameter-free DFT approach (Sec. II).

To calculate the temperature dependence of the magnetization, we use the RPA method as described in the appendix. We consider both classical-spin and quantum-spin cases.
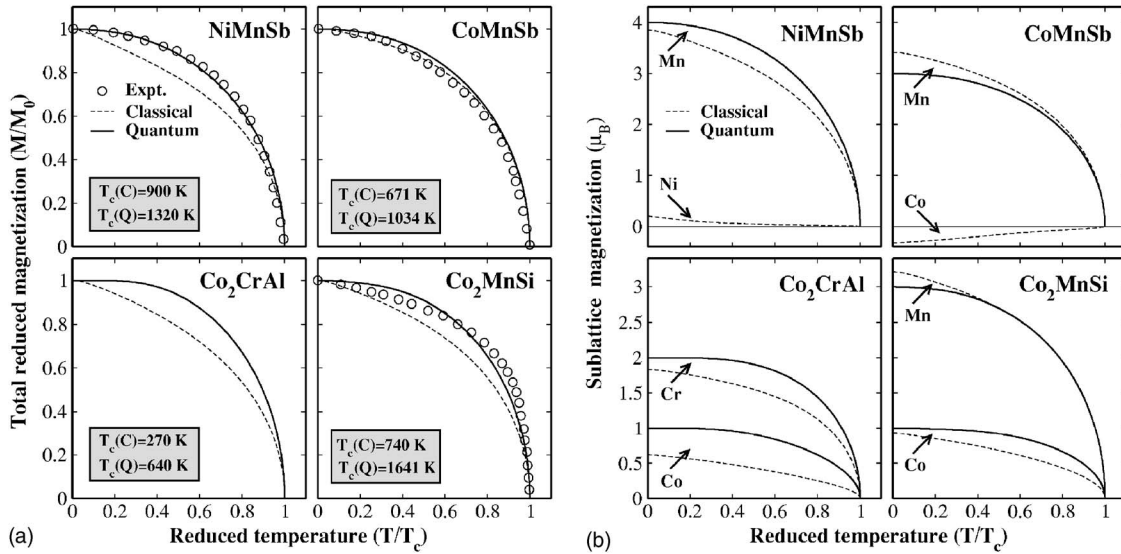
FIG. 7. (a) The calculated temperature dependence of the total magnetization for both families of Heusler alloys. For comparison the experimental temperature dependences (Ref. 12) are presented. The calculations are performed for both classical and quantum Hamiltonians. Both the magnetization and the temperature are given in reduced form. (b) Calculated sublattice magnetizations as a function of temperature. The temperature is given in reduced form.

In the classical-spin calculations, the calculated values of the magnetic moments (Table I) are used. To perform the quantum-mechanical RPA calculation, we assign integer values to the atomic moments. In the semi-Heusler compounds, we ignore the induced moments on Ni and Co atoms and assign the whole moment per formula unit to the Mn atom: $4\mu_B(S=2)$ in NiMnSb and $3\mu_B(S=3/2)$ in CoMnSb. In Co_2MnSi, we take the values of $3\mu_B(S=3/2)$ and $1\mu_B(S=1/2)$ for Mn and Co atoms, respectively. This assignment preserves the value of the total spin moment per chemical unit. In Co_2CrAl, we use in the quantum-RPA calculations the atomic moment of $2\mu_B(S=1)$ for Cr and $1\mu_B(S=1/2)$ for Co.

In Fig. 7(a), we present in the normalized form, the calculated temperature dependence of the magnetization for both families of Heusler compounds. The calculations are performed for the experimental lattice parameter. For comparison, the experimental curves are presented. The nature of the spin (quantum or classical) influences the form of the curves considerably. The classical curve lies lower than the quantum one. This results from a faster drop of the magnetization in the low-temperature region in the case of classical spins. In general, the quantum consideration gives better agreement of the form of the temperature dependence of the magnetization with experiment.

In Fig. 7(b), we present the temperature dependence of the magnetization of individual sublattices. As expected from the previous discussions in half-Heusler systems, the main contribution to the magnetization comes from the Mn sublattice while for the full-Heusler systems, both 3*d* atoms contribute substantially.

Considering the calculated Curie temperatures, we notice that the value of T_C calculated within the quantum-mechanical RPA is substantially larger than the corresponding classical estimation (see Fig. 7). This property is well

known and has its mathematical origin in the factor $(S+1)/S$ entering the RPA expression for the Curie temperature [Eq. (A14)]. In Fig. 8, we show the dependence of the Curie temperature calculated within the quantum-mechanical RPA approach on the value of S. The exchange parameters are kept unchanged in these calculations. We see that the dependence has a monotonous character tending to a classical limit for large S.

Presently, we do not have an explanation why quantum-mechanical calculations give better form of the temperature dependence while the classical calculation provides better value of the Curie temperature. We can suggest the following arguments. The quantum treatment is more appropriate than the classical one in the low-temperature region. At high tem-
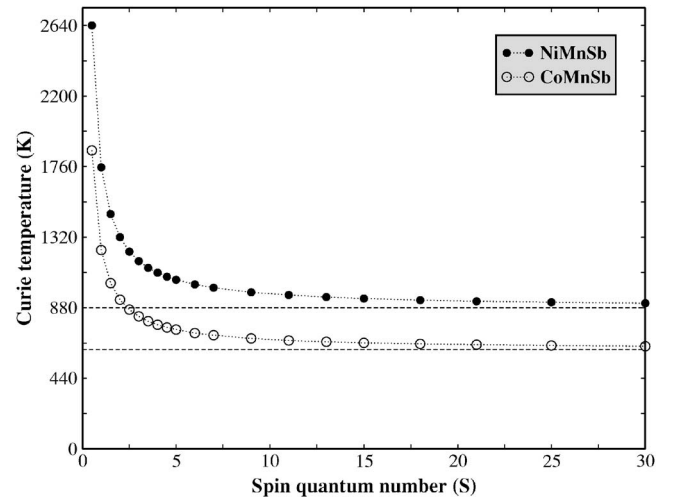

FIG. 8. Curie temperature of NiMnSb and CoMnSb as a function of spin quantum number S. The horizontal broken lines correspond to the classical limit ($S=\infty$).

peratures characterized by strong deviation of the atomic spins from the magnetization axis, the quantum treatment gives too slow decrease of the magnetization. It is worth noting that the consequent theory should take into account not only the orientational disorder of the atomic moments, but also the single-particle (Stoner-type) excitations leading to the decrease of atomic moments. Another important aspect is related to the fact that the exchange parameters used in the calculations are estimated within the picture of classical atomic moments described above. It is possible that the values of the exchange parameters must be modified for the use in the quantum-mechanical case. These questions belong to fundamental problems of the quantum-mechanical description of the magnetic systems with itinerant electrons.

VI. SUMMARY AND CONCLUSIONS

We studied the electronic structure of several Heusler alloys using the augmented spherical waves method in conjunction with the generalized gradient approximation to the exchange and correlation potential. Using the frozen-magnon approximation, we calculated interatomic exchange parameters that were used to estimate the Curie temperature. The Curie temperature was estimated within both mean-field and random-phase approximation techniques.

For the half-Heusler alloys, NiMnSb and CoMnSb, the dominant interaction is between the Mn atoms. The lattice compression results in considerable change of the exchange parameters and Curie temperature.

The magnetic interactions are more complex in full-Heusler alloys Co_2MnSi and Co_2CrAl. In both cases, the ferromagnetism is stabilized by the intersublattice interactions between the Mn(Cr) and Co atoms and between Co atoms belonging to different sublattices. Both the random-phase and mean-field approximations slightly underestimate the values of the Curie temperature. Compression of the lattice constant has little effect on the magnetic properties of the full-Heusler alloys.

We study the temperature dependence of the magnetization within the quantum mechanical and classical RPA. The quantum-mechanical approach gives the form of the temperature dependence that is in good agreement with experiment. The value of the Curie temperature is, however, overestimated in the quantum-mechanical calculation.

ACKNOWLEDGMENTS

APPENDIX: THE RANDOM-PHASE APPROXIMATION FOR THE MULTISUBLATTICE HEISENBERG HAMILTONIAN

The Green's function approach is a powerful tool in the study of the magnetism of complex systems. (See, e.g., the application of the method to antiferromagnets,[37]

ferrimagnets,[38,39] random alloys,[40] layered systems,[41–43] disordered dilute magnetic systems,[44] and multisublattice ferromagnets.[45]) In this appendix, we briefly overview the formalism to study the temperature dependence of the magnetization of multisublattice systems within the random-phase approximation.

We start with the Heisenberg Hamiltonian for quantum spins

$$H = -\sum_{ij} \sum_{\mu\nu} J_{ij}^{\mu\nu} \mathbf{e}_{i,\mu} \mathbf{e}_{j,\nu}, \qquad (A1)$$

where $\mathbf{e}_{i,\mu} = (\hat{s}_{i,\mu}^x, \hat{s}_{i,\mu}^y, \hat{s}_{i,\mu}^z)/(S_\mu)$ is the normalized spin operator corresponding to site (i,μ).

In terms of the creation and destruction operators $\hat{s}_{i,\mu}^{\mp} = \hat{s}_{i,\mu}^x \mp \hat{s}_{i,\mu}^y$ the Hamiltonian can be written in the form

$$H = -\sum_{ij} \sum_{\mu\nu} \tilde{J}_{ij}^{\mu\nu} [\hat{s}_{i,\mu}^+ \hat{s}_{j,\nu}^- + \hat{s}_{i,\mu}^z \hat{s}_{j,\nu}^z], \qquad (A2)$$

where $\tilde{J}_{ij}^{\mu\nu} = J_{ij}^{\mu\nu}/S_\mu S_\nu$.

Following Callen,[34] let us introduce the Green's function

$$G_{ij}^{\mu\nu}(\tau) = -\frac{i}{\hbar} \theta(\tau) \langle [\hat{s}_{i,\mu}^+(\tau), \exp(\eta \hat{s}_{j,\nu}^z) \hat{s}_{j,\nu}^-] \rangle, \qquad (A3)$$

where η is a parameter, $\theta(\tau)$ is the step function $[\theta(\tau)=1$ for $\tau \geq 0]$, $[\ldots]$ denotes the commutator and $\langle \ldots \rangle$ is the thermal average over the canonical ensemble, i.e., $\langle F \rangle = \mathrm{Tr}[\exp(-\beta H)F]/\mathrm{Tr}[\exp(-\beta H)]$ with $\beta = 1/k_B T$.

Writing the equation of motion for $G_{ij}^{\mu\nu}(\tau)$, we obtain

$$\frac{\partial}{\partial \tau} G_{ij}^{\mu\nu}(\tau) = -\frac{i}{h} \delta(\tau) \langle [\hat{s}_{i,\mu}^+(\tau), \exp(\eta \hat{s}_{j,\nu}^z) \hat{s}_{j,\nu}^-] \rangle - \frac{1}{\hbar^2} \theta(\tau)$$

$$\times \langle [[\hat{s}_{i,\mu}^+(\tau), \hat{H}], \exp(\eta \hat{s}_{j,\nu}^z) \hat{s}_{j,\nu}^-] \rangle. \qquad (A4)$$

The last commutator term in Eq. (A4) generates higher-order Green's functions. These functions can be reduced to lower-order functions by using Tyablikov decoupling (random-phase approximation) scheme[33]

$$\langle [\hat{s}_{i,\mu}^+(\tau) \hat{s}_{k,\mu}^z, \hat{s}_{j,\nu}^-] \rangle \approx \langle \hat{s}_{k,\mu}^z \rangle \langle [\hat{s}_{i,\mu}^+(\tau), \hat{s}_{j,\nu}^-] \rangle. \qquad (A5)$$

Applying this decoupling procedure to Eq. (A4), we get

$$\frac{\partial}{\partial \tau} G_{ij}^{\mu\nu}(\tau) = -\frac{i}{h} \delta(\tau) \langle [\hat{s}_{i,\mu}^+(\tau), \exp(\eta \hat{s}_{j,\nu}^z) \hat{s}_{j,\nu}^-] \rangle$$

$$+ \frac{2i}{\hbar} \sum_{k,\xi} \tilde{J}_{i,k}^{\mu\xi} [\langle \hat{s}_{i,\mu}^z \rangle G_{kj}^{\xi\nu}(\tau) - \langle \hat{s}_{k,\xi}^z \rangle G_{ij}^{\mu\nu}(\tau)]. \qquad (A6)$$

After a Fourier transformation to energy and momentum space $[g(\mathbf{q}, \omega) = 1/2\pi \Sigma_l \int d\omega e^{-i\mathbf{q}\mathbf{R}_l} G_{l0}(\tau)]$, we obtain

$$\hbar \omega g_{\mu\nu}(\mathbf{q}, \omega) = \frac{1}{2\pi} \langle [\hat{s}_\mu^+, \exp(\eta \hat{s}_\nu^z) \hat{s}_\nu^-] \rangle \delta_{\mu\nu} - 2 \sum_\xi \{ \tilde{J}_{\mu\xi}(\mathbf{q})$$

$$\times \langle \hat{s}_{i,\mu}^z \rangle g_{\xi\nu}(\mathbf{q}, \omega) - \tilde{J}_{\mu\xi}(0) \langle \hat{s}_{k,\xi}^z \rangle g_{\mu\nu}(\mathbf{q}, \omega) \}. \qquad (A7)$$

Eq. (A7) can be written in a compact matrix form

$$[\hbar\omega\mathbf{I} - \mathbf{M}(\mathbf{q})]\mathbf{g}(\mathbf{q},\omega) = \mathbf{u}, \qquad (A8)$$

where $\mathbf{g}(\mathbf{q},\omega)$ is a symmetric square matrix, $\mathbf{I}$ is a unit matrix, and the inhomogeneity matrix $\mathbf{u}$ is expressed by

$$u_{\mu\nu} = \frac{1}{2\pi}\langle[\hat{s}_\mu^+, \exp(\eta\hat{s}_\nu^z)\hat{s}_\nu^-]\rangle\delta_{\mu\nu}, \qquad (A9)$$

matrix $\mathbf{M}(\mathbf{q})$ is defined by

$$M_{\mu\nu}(\mathbf{q}) = \left\{\sum_\xi 2\tilde{J}_{\mu\xi}(\mathbf{0})\langle\hat{s}_\xi^z\rangle\right\}\delta_{\mu\nu} - 2\tilde{J}_{\mu\nu}(\mathbf{q})\langle\hat{s}_\mu^z\rangle. \quad (A10)$$

Next, we introduce the transformation which diagonalizes matrix $\mathbf{M}(\mathbf{q})$,[43]

$$\mathbf{L}(\mathbf{q})\mathbf{M}(\mathbf{q})\mathbf{R}(\mathbf{q}) = \Omega(\mathbf{q}), \qquad (A11)$$

where $\Omega(\mathbf{q})$ is the diagonal matrix whose elements give the spin-wave energies $\omega_\mu(\mathbf{q})$. The number of branches in the spin-wave spectrum is equal to the number of magnetic atoms in the unit cell. The transformation matrix $\mathbf{R}(\mathbf{q})$ and its inverse $\mathbf{R}^{-1}(\mathbf{q}) = \mathbf{L}(\mathbf{q})$ are obtained from the right eigenvectors of $\mathbf{M}(\mathbf{q})$ as columns and from the left eigenvectors as rows, respectively.

Using the spectral theorem and Callen's technique,[34] one obtains the thermal averages of the sublattice magnetizations

$$\langle\hat{s}_\mu^z\rangle = \frac{(S_\mu - \Phi_\mu)(1 + \Phi_\mu)^{2S_\mu+1} + (S_\mu + 1 + \Phi_\mu)\Phi_\mu^{2S_\mu+1}}{(1 + \Phi_\mu)^{2S_\mu+1} - (\Phi_\mu)^{2S_\mu+1}}, \qquad (A12)$$

where Φ_μ is an auxiliary function given by

$$\Phi_\mu = \frac{1}{N}\sum_q\sum_\nu L_{\mu\nu}(\mathbf{q})\frac{1}{e^{\beta\omega_\nu(\mathbf{q})} - 1}R_{\mu\nu}(\mathbf{q}). \qquad (A13)$$

In Eq. (A13), N is the number of $\mathbf{q}$ points in the first BZ.

Equation (A12) is the central equation for the calculation of the sublattice magnetizations. It must be solved self-consistently. The Curie temperature T_C is determined as the point where all sublattice magnetizations vanish.

Near T_C ($\Phi_\mu\rightarrow\infty$ and $\langle\hat{s}_\mu^z\rangle\rightarrow 0$), Eq. (A12) can be simplified. Expanding in Φ_μ and using Eq. (A13), one obtains

$$\langle\hat{s}_\mu^z\rangle = \frac{(S_\mu+1)}{3S_\mu}\left\{\frac{1}{S_\mu^2 N}\sum_{q,\nu}L_{\mu\nu}(\mathbf{q})\frac{1}{e^{\beta\omega_\nu(\mathbf{q})} - 1}R_{\mu\nu}(\mathbf{q})\right\}^{-1}. \qquad (A14)$$

From Eq. (A14), it follows that for spin-independent Heisenberg exchange parameters [Eq. (A1)] the dependence of the Curie temperature on the spin value is defined by the factor $(S_\mu+1)/S_\mu$.

The classical limit can be obtained by letting $S_\mu\rightarrow\infty$ in Eqs. (A12) and (A14).[45] Factor $(S_\mu+1)/S_\mu$ in Eq. (A14) becomes in this case unity. The temperature dependence of the magnetization can be calculated using a semiclassical analog of Eq. (A12) given by[45,52]

$$\langle e_\mu^z\rangle = \mathcal{L}\left(\left\{\frac{1}{N}\sum_{q,\nu}L_{\mu\nu}(\mathbf{q})\frac{1}{e^{\beta\omega_\nu(\mathbf{q})} - 1}R_{\mu\nu}(\mathbf{q})\right\}^{-1}\right), \qquad (A15)$$

where $\mathcal{L}(x) = \coth(x) - 1/x$ is the Langevin function and $\mathbf{e}_\mu$ is the angular momentum vector of size one.

---

*Electronic address: ersoy@mpi-halle.de

†Electronic address: lsandr@mpi-halle.de

‡Electronic address: bruno@mpi-halle.de

§Electronic address: i.galanakis@fz-juelich.de

[1] I. Žutić, J. Fabian, and S. Das Sarma, Rev. Mod. Phys. **76**, 323 (2004).

[2] J. de Boeck, W. van Roy, J. Das, V. Motsnyi, Z. Liu, L. Lagae, H. Boeve, K. Dessein, and G. Borghs, Semicond. Sci. Technol. **17**, 342 (2002).

[3] R. A. de Groot, F. M. Mueller, P. G. van Engen, and K. H. J. Buschow, Phys. Rev. Lett. **50**, 2024 (1983).

[4] I. Galanakis, P. H. Dederichs, and N. Papanikolaou, Phys. Rev. B **66**, 134428 (2002).

[5] S. Ishida, S. Akazawa, Y. Kubo, and J. Ishida, J. Phys. F: Met. Phys. **12**, 1111 (1982); S. Ishida, S. Fujii, S. Kashiwagi, and S. Asano, J. Phys. Soc. Jpn. **64**, 2152 (1995).

[6] I. Galanakis, P. H. Dederichs, and N. Papanikolaou, Phys. Rev. B **66**, 174429 (2002).

[7] S. Fujii, S. Ishida, and S. Asano, J. Phys. Soc. Jpn. **64**, 185 (1995); I. Galanakis, J. Phys.: Condens. Matter **16**, 3089 (2004); S. Ishida, T. Masaki, S. Fujii, and S. Asano, Physica B **245**, 1 (1998); Y. Miura, K. Nagao, and M. Shirai, Phys. Rev. B **69**, 144413 (2004); J. Tobola and J. Pierre, J. Alloys Compd. **296**, 243 (2000); R. Weht and W. E. Pickett, Phys. Rev. B **60**, 13006

(1999); M. Zhang, X. Dai, H. Hu, G. Liu, Y. Cui, Z. Liu, J. Chen, J. Wang, and G. Wu, J. Phys.: Condens. Matter **15**, 7891 (2003); M. Zhang, Z. Liu, H. Hu, G. Liu, Y. Cui, G. Wu, E. Brück, F. R. de Boer, and Y. Li, J. Appl. Phys. **95**, 7219 (2004); W. H. Wang, M. Przybylski, W. Kuch, L. I. Chelaru, J. Wang, Y. F. Lu, J. Barthel, H. L. Meyerheim, and J. Kirschner, Phys. Rev. B **71**, 144416 (2005); S. J. Hashemifar, P. Kratzer, and M. Scheffler, Phys. Rev. Lett. **94**, 096402 (2005); I. Galanakis, M. Ležaić, G. Bihlmayer, and S. Blügel, Phys. Rev. B **71**, 214431 (2005).

[8] H. Akinaga, T. Manago, and M. Shirai, J. Phys. Soc. Jpn. **39**, L1118 (2000).

[9] R. J. Soulen Jr., J. M. Byers, M. S. Osofsky, B. Nadgorny, T. Ambrose, S. F. Cheng, P. R. Broussard, C. T. Tanaka, J. Nowak, J. S. Moodera, A. Barry, and J. M. D. Coey, Science **282**, 85 (1998).

[10] A. Stroppa, S. Picozzi, A. Continenza, and A. J. Freeman, Phys. Rev. B **68**, 155203 (2003).

[11] H. Akai, Phys. Rev. Lett. **81**, 3002 (1998).

[12] P. J. Webster and K. R. A. Ziebeck, in *Alloys and Compounds of d-Elements with Main Group Elements. Part 2.*, edited by H. P. J. Wijn, Landolt-Boörnstein, New Series, Group III, Vol. 19, Pt. C (Springer-Verlag, Berlin, 1988), pp. 75–184.

[13] B. R. K. Nanda and S. Dasgupta, J. Phys.: Condens. Matter **15**,

7307 (2003).

[14] L. Chioncel, M. I. Katsnelson, R. A. de Groot, and A. I. Lichtenstein, Phys. Rev. B **68**, 144425 (2003).

[15] T. Block, M. J. Carey, B. A. Gurney, and O. Jepsen, Phys. Rev. B **70**, 205114 (2004).

[16] S. Picozzi, A. Continenza, and A. J. Freeman, Phys. Rev. B **66**, 094421 (2002); I. Galanakis, S. Ostanin, M. Alouani, H. Dreyssé, and J. M. Wills, Phys. Rev. B **61**, 4093 (2000).

[17] Ph. Mavropoulos, K. Sato, R. Zeller, P. H. Dederichs, V. Popescu, and H. Ebert, Phys. Rev. B **69**, 054424 (2004); Ph. Mavropoulos, I. Galanakis, V. Popescu, and P. H. Dederichs, J. Phys.: Condens. Matter **16**, S5759 (2004).

[18] I. Galanakis, Phys. Rev. B **71**, 012413 (2005).

[19] P. Larson, S. D. Mahanti, and M. G. Kanatzidis, Phys. Rev. B **62**, 12754 (2000).

[20] D. Orgassa, H. Fujiwara, T. C. Schulthess, and W. H. Butler, Phys. Rev. B **60**, 13237 (1999).

[21] S. Picozzi, A. Continenza, and A. J. Freeman, Phys. Rev. B **69**, 094423 (2004).

[22] P. A. Dowben and R. Skomski, J. Appl. Phys. **93**, 7948 (2003); **95**, 7453 (2004).

[23] J. Kübler, A. R. Williams, and C. B. Sommers, Phys. Rev. B **28**, 1745 (1983).

[24] E. Şaşıoğlu, L. M. Sandratskii, and P. Bruno, Phys. Rev. B **70**, 024427 (2004); E. Şaşıoğlu, L. M. Sandratskii, and P. Bruno, Phys. Rev. B **71**, 214412 (2005); E. Şaşıoğlu, L. M. Sandratskii, and P. Bruno, J. Magn. Magn. Mater. **290–291**, 385 (2005).

[25] E. Şaşıoğlu, L. M. Sandratskii, and P. Bruno, J. Phys.: Condens. Matter **17**, 995 (2005).

[26] Y. Kurtulus, R. Dronskowski, G. D. Samolyuk, and V. P. Antropov, Phys. Rev. B **71**, 014425 (2005).

[27] J. Kübler, Phys. Rev. B **67**, 220403(R) (2003).

[28] A. R. Williams, J. Kübler, and C. D. Gelatt, Phys. Rev. B **19**, 6094 (1979).

[29] O. K. Andersen, Phys. Rev. B **12**, 3060 (1975).

[30] J. P. Perdew and Y. Wang, Phys. Rev. B **45**, 13244 (1992).

[31] N. M. Rosengaard and B. Johansson, Phys. Rev. B **55**, 14975 (1997); S. V. Halilov, H. Eschrig, A. Y. Perlov, and P. M. Oppeneer, Phys. Rev. B **58**, 293 (1998); L. M. Sandratskii and P. Bruno, Phys. Rev. B **67**, 214402 (2003).

[32] P. W. Anderson, in *Solid State Physics*, edited by F. Seitz and D. Turnbull (Academic Press, New York), Vol. 14, pp. 99–214.

[33] S. V. Tyablikov, *Methods of Quantum Theory of Magnetism* (Plenum Press, New York, 1967).

[34] H. B. Callen, Phys. Rev. **130**, 890 (1963).

[35] M. Pajda, J. Kudrnovsky, I. Turek, V. Drchal, and P. Bruno, Phys. Rev. B **64**, 174402 (2001).

[36] G. Bouzerar, J. Kudrnovský, L. Bergqvist, and P. Bruno, Phys. Rev. B **68**, 081203(R) (2003).

[37] M. E. Lines, Phys. Rev. **135**, A1336 (1964); D. A. Yablonskiy, Phys. Rev. B **44**, 4467 (1991); Qing'an Li, Phys. Rev. B **70**, 014406 (2004).

[38] D. L. Lin and Hang Zheng, Phys. Rev. B **37**, 5394 (1988); H. Zheng and D. L. Lin, Phys. Rev. B **37**, 9615 (1988); Jun Li, An Du, and Guozhu Wei, Physica B **348**, 79 (2004); Rong-ke Qiu and Zhi-dong Zhang, J. Phys.: Condens. Matter **13**, 4165 (2001); Rong-ke Qiu and Zhi-dong Zhang, Phys. Status Solidi B **241**, 189 (2003).

[39] R. E. Mills, R. P. Kenan, and F. J. Milford, Phys. Lett. **12**, 173 (1964); Roger E. Mills, Richard P. Kenan, and Frederick J. Milford, Phys. Rev. **145**, 704 (1966).

[40] P. Azaria and T. Diep, J. Appl. Phys. **61**, 4422 (1987).

[41] V. T. Ngo, H. V. Nguyen, H. T. Diep, and V. L. Nguyen, Phys. Rev. B **69**, 134429 (2004); Rong-ke Qiu and Zhi-dong Zhang, J. Phys.: Condens. Matter **14**, 3259 (2002).

[42] Diep-The-Hung, J. C. S. Levy, and O. Nagai, Phys. Status Solidi B **93**, 351 (1979); Wenli Guo, L. P. Shi, and D. L. Lin, Phys. Rev. B **62**, 14259 (2000).

[43] P. Fröbrich, P. J. Jensen, P. J. Kuntz, and A. Ecker, Eur. Phys. J. B **18**, 579 (2001); P. Fröbrich and P. J. Kuntz, Phys. Rev. B **68**, 014410 (2003).

[44] S. Hilbert and W. Nolting, Phys. Rev. B **70**, 165203 (2004); S. Hilbert and W. Nolting, Phys. Rev. B **71**, 113204 (2005).

[45] J. Rusz, I. Turek, and M. Diviš, Phys. Rev. B **71**, 174408 (2005).

[46] E. Şaşıoğlu, I. Galanakis, L. M. Sandratskii, and P. Bruno, J. Phys.: Condens. Matter **17**, 3915 (2005).

[47] E. Şaşıoğlu, L. M. Sandratskii, and P. Bruno, J. Appl. Phys. **98**, 063523 (2005).

[48] R. F. Sabiryanov and S. S. Jaswal, Phys. Rev. Lett. **79**, 155 (1997).

[49] *Half-metallic Alloys-Fundamentals and Applications*, Lecture Notes in Physics, Vol. **676**, I. Galanakis and P. H. Dederichs (eds.), (Springer-Berlin, Heidelberg 2005), pp. 1–39; cond-mat/0408068 (unpublished).

[50] S. Plogmann, T. Schlathölter, J. Braun, M. Newmann, Y. M. Yarmoshenko, M. V. Yablonskikh, E. I. Shreder, E. Z. Kurmaev, A. Wrona, and A. Ślebarski, Phys. Rev. B **60**, 6428 (1999).

[51] N. David Mermin, Phys. Rev. **137**, A1441 (1965).

[52] H. B. Callen and S. Shtrikman, Solid State Commun. **3**, 5 (1965).